INFLUENCE OF NON-UNIFORM WALL TEMPERATURE ON LOCAL HEAT TRANSFER COEFFICIENT IN A ROTATING SQUARE CHANNEL

Kazem Farhadi

Abstract: This paper presents the results of an experimental examination of the effect of non-uniform wall temperature on local heat transfer coefficient in a rotating smooth-walled square channel. Three different thermal boundary situations were investigated: (a) even and odd (four) wall uniform temperature, (b) even and odd (four) wall uniform heat flux, and (c) even (leading and trailing) walls hot with two side walls kept cold. It is demonstrated that the local heat transfer coefficients on the trailing edge are much higher than that of the leading edge. For situation (a) of even (leading and trailing) walls with two sides uniform temperature, the leading edge heat transfer coefficient decreases and then increases with increasing rotational numbers. And the trailing edge heat transfer coefficient increases monotonically with rotational numbers increasing. However, the trailing edge as well as the side walls heat transfer coefficient for situation (b) is higher than situation (a) and the leading edge local heat transfer coefficients for situations (b) and (c) are significantly higher than situation (a). The obtained results suggest that the local non-uniform wall temperature creates the local buoyancy force that diminishes the effect of the Coriolis force. Consequently, the local heat transfer coefficients on leading, trailing, and side edges are affected by the wall non-uniform temperature.

1. Introduction

The aircraft engine designer seeks for his engines to operate better in three basic respects. To give more thrust, to have less weight, and to require less fuel.

The intention in advanced aero-engine design for high thermal efficiency and high power density is toward high entry gas temperature. However, in most practical aero-gas engine the entry gas temperature is far above the permitted metal temperature. Consequently, very high sophisticated cooling technologies such as film cooling, impingement cooling, and extended surfaces convection cooling ought to be in order to maintain the structural integrity of blades and vanes employed in advanced gas turbine engines. Since heat is transferred both from the pressure and suction edges, rib promoter are often cast on two opposite walls of the cooling passages. A typical coolant passage can be modeled as a single pass or multi-pass rectangular channel with even and odd (leading and trailing edges with two sides) walls or with two opposite rib-roughened walls.

The majority of existing experimental data on internally cooling blade channel are reported to be from the tests accomplished with non-rotating flow condition [1], [2], [3], and [4]. Rotation of turbine blade cooling channels results in Coriolis and buoyancy forces. In turn, these forces could significantly alter coolant flow patterns and influence the local heat transfer distribution. Needless to say that heat transfer experimental data are expensive to achieve, particularly under rotation. Hence, merely limited data is available in the open literature. Possibly the first work with rotation is attributed to Mori et al., [5] who studied the mean forced convective heat transfer in a rotating radial circular tube.

Clifford et al., [6] announced the local and mean heat transfer in a triangular-sectioned channel rotating in the orthogonal mode. Morris et al., [7, 8, 9, and 10] investigated the effect of rotation on the local heat transfer coefficient of circular, triangular, rectangular, and internally ribbed circular sectioned coolant channels of turbine rotor blades. Song [11] presented the study of forced convective heat transfer in a rotating coolant channel. Lieu et al., [12] studied local heat transfer coefficient in a rotating coolant passage with artificially roughened walls (leading and trailing edges). On the other hand, Wagner et al., [13, 14, 15, and 16] studied

the local heat transfer in rotating serpentine passages with smooth-walled and two opposite roughened walls (leading and trailing edges). All the aforementioned experimental work was conducted with smooth walled channels but the work of Liou [12], Wagner [13, 16], and Clifford [6].

Exceptionally, the works of Wagner [15, 16] were conducted on the channels other than smooth walled. In the late 1990, the researchers were concentrated on new techniques for cooling channels design. For example Matsuda, H. et al [17] used a thermo chromic liquid crystal for temperature identification. He used this liquid crystal to apply for film cooling effectiveness measurements. Saekei [18] also applied liquid crystal for measurements on turbine nozzle. Later on the working fluid changes from ordinary water to carbon dioxide [19]. Saeki [20] worked on heat transfer measurements on a gas turbine blade cooling and compared against liquid crystal results which was obtained previously. He believed that heat transfer measurements with crystal liquid produced more accurate results compared with water. In fact using the unique thermo chromic liquid crystal technique, which utilizes the color information of a liquid crystal to estimate temperature, performed the measurement of the heat transfer coefficient. The blade surface heat transfer coefficient was calculated from heat flux and temperature. Heat flux of the blade surface was estimated from metal foil heater energy input, considering the inter-solid heat loss calculated by heat conduction analysis.

Blade surface temperature has been converted from video recorded color of the liquid crystal. Shoko [21] measured heat transfer coefficient of the smooth wall channel agreed well with the turbulent channel correlation. And the rib effect was measured by the ratio of the Nussle number to that of the smooth wall condition.

It was found that the rib surface heat transfer for the broken rib was about 2.0 to 2.3 times higher than that for the continuous rib. This leads to the conclusion that the broken rib heat transfer enhancement comes from the rib surface thermal boundary layer thinning effect. Some researchers concluded that large increases and decreases in trailing and leading edges heat transfer coefficients were found to take place under certain conditions of rotational situation. On the other hand, some other researchers found lesser effects. However, as one would expect, there could be some inconsistencies exist between the results of researchers that is due to different methods used for measurements, physical models, and channel test section physical and geometrical conditions. The local heat transfer coefficient on the trailing edge due to rotation can be increased up to 3.5 times as compared to non-rotating fully developed smooth walled channel values. However, the leading edge local heat transfer coefficient can be decreased up to 40 percent of the fully developed circular-sectioned channel values. The local heat transfer coefficient on the trailing edge, of the first coolant passage and with radial outward flow direction, increases with increasing rotational speed and

wall-to-coolant temperature difference. It is believed that this is because the rotation induces the thinner destabilization boundary layer on the trailing edge and the buoyancy causes the near wall counter-flow interaction with the mainstream on the trailing edge of the first coolant passage (see Fig. 1 for clarity).
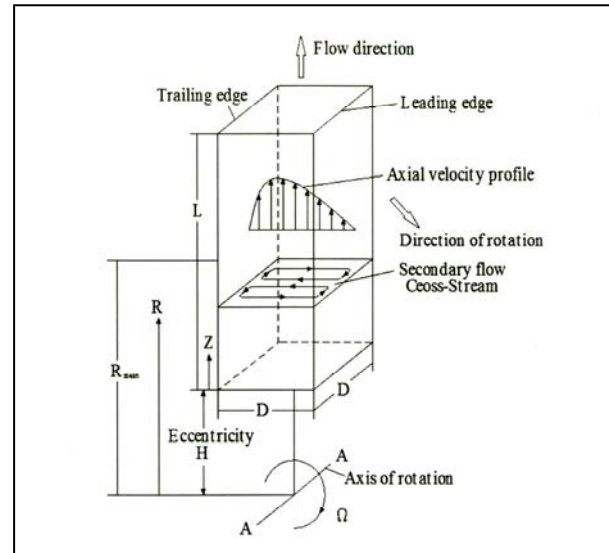

Fig 1. Conceptual view of coolant flow distribution (orthogonal-mode rotation)

Since the cross-stream secondary flow and buoyancy-induced near-wall turbulence are very sensitive to wall thermal boundary conditions, it is of interest to study the effects of different wall heating conditions on the leading and trailing edge of the first coolant passage under rotational conditions (see Fig. 2)
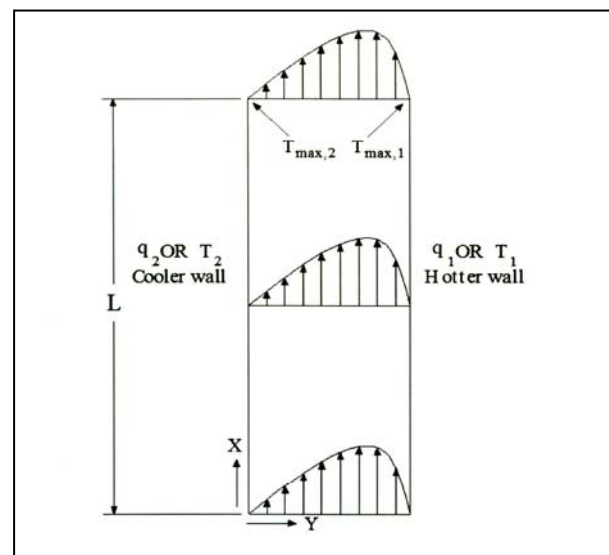

Fig 2. Conceptual view of flow model

The objective of the present work is to study the effect of wall heating condition on the local heat transfer coefficient in a rotating square smooth walled channel

with radial outward flow direction. Therefore, three surface heating conditions were tested, namely: (1) four wall uniform temperature.

This could be used as a baseline test to compare the experimental data of Boelter et al., [22]. (2) Four wall uniform heat flux. This could be used as another baseline test to compare the data of four walls uniform temperature. (3) Leading and trailing edges heated to the same temperature but with two sides walls unheated. It is worth to note that among these three thermal boundary conditions, (1) and (2) are typical reference cases, whereas, (3) simulate turbine engine conditions. The boundary conditions (1), (2), and (3) are referred to as situations (a), (b), (c), respectively.

The experimental results of uniform wall temperature, situation (a) are compared to the previous data Wagner et al., [14] at the similar rotational number and buoyancy forces. This was compared to those with non-uniform wall temperature situation (b) and (c). The effect of wall heating conditions situation (a), (b), and (c) on the local heat transfer coefficient, i.e., leading, trailing, and side edges are then identified by similar rotational speed and Reynolds number.

2. Experimental Setup
2.1. Rotating Facility
The mechanical layout of the rotating test facility into which the test module was fitted is shown in Fig. 3.
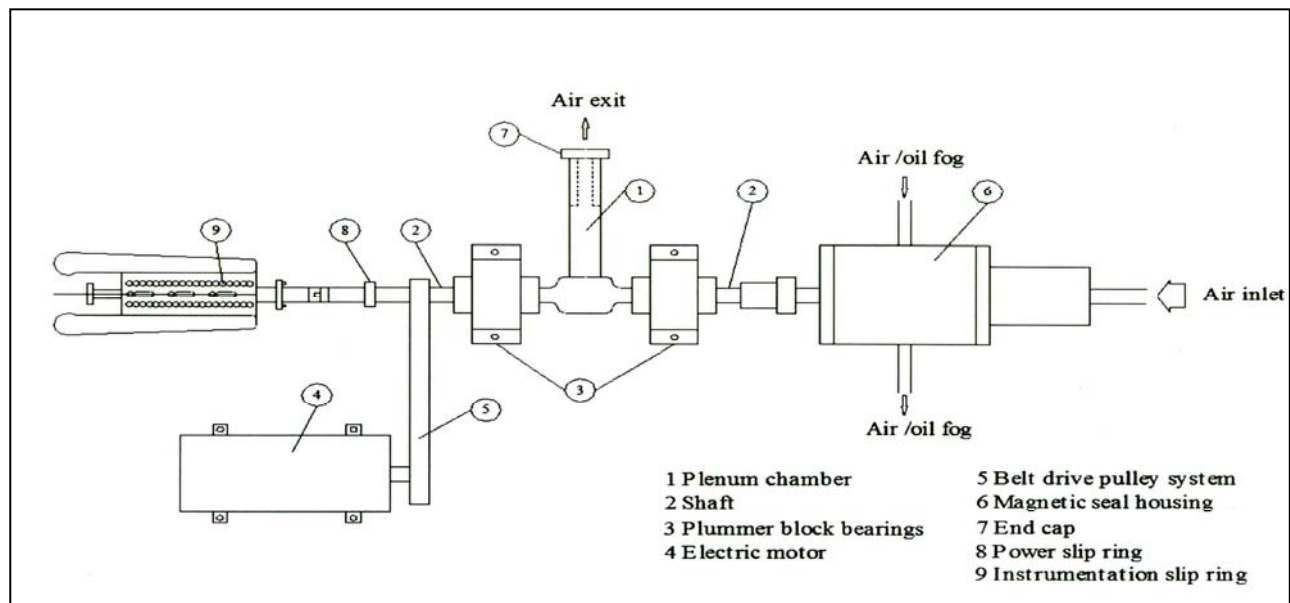

Fig 3. Schematic of the test facility

A hollow air delivery plenum chamber (1) was bolted to a shaft (2), which itself was supported between two Plummer block bearing (3). The shaft/plenum chamber assembly was derived by means of a controllable electric motor (4) via a toothed belt drive pulley system (5). The right-hand side of the shaft, as viewed in the figure, was bored to permit the passage of air to the plenum chamber and hence to the actual instrumented test geometry (6) used. A compressor was used to supply compressed air into the test section. The test model, a two-pass square channel with a sharp 180 degree turn, is fitted into the plenum at a specified eccentricity to the axis of rotation. To simulate engine configuration, the ratio of the mean rotating arm radius to the channel hydraulic diameter ratio is 30. A rotary seal (7), fitted over the extreme right hand end of the shaft assembly, allowed pressurized air to be fed to the plenum chamber and hence through the test section assembly, finally exhausting to atmosphere. An electrical two channels power slip ring (8) permitted current from a Varied transformer supply to be fed to the heater section with the heater power consumption being

measured with a conventional wattmeter. A silver/silver-graphite multi-channel instrumentation slip ring (9) was used to take the thermocouple signals from the experimental set up to a Schlumberger Orion data acquisition system and a magnetic encoder and timer counter fitted to this slip ring permitted the speed of the rotor to be measured.

The instrumented dry and oil free air from a central laboratory facility could be fed to the rotary seal inlet and monitored via an Annular differential pressure flow meter. Valves located upstream of the rotating facility permitted the control of the airflow through the test module. In order to obtain an actually regional averaged heat transfer coefficients for aero-gas turbine cooling channel design, it is preferable to have a test section that can determine regionally averaged heat transfer coefficients in the channel stream-wise flow direction. The two-pass square channel is divided into twelve small copper sections. The instrumented two-pass square channel is shown in Fig. 4. Each copper section is comprised four copper plates. To minimize possible heat

conduction, thin Teflon strips are machined along the periphery contract surface between copper sections as insulation. The local wall temperature of the test module is measured by constantan thermocouples distributed along the length and across the circumference of the copper duct. The inlet air temperature was measured with a thermocouple at the inlet central plane of the heated smooth walled channel. There is an unheated Teflon entrance region that has the same cross-section and length as that of the test module. This entry length duct serves to establish fully developed flow at the entrance to the test module. The cross-section of the test module is shown in figure 4. The orientation of the test module is such that the leading and trailing walls of the square cross-sections are vertical and the two opposite sidewalls are horizontal. The resistance heaters are uniformly cemented between the copper plate back-face grooves and the Teflon wall to insure good contact. Individual of the four channel walls has its own heater with each heater controlled by a Varian transformer independently. In this way, each heater supplies a controllable heat flux for each channel wall. The smooth sidewalls are isolated from the leading and trailing walls to eliminate heat conduction.
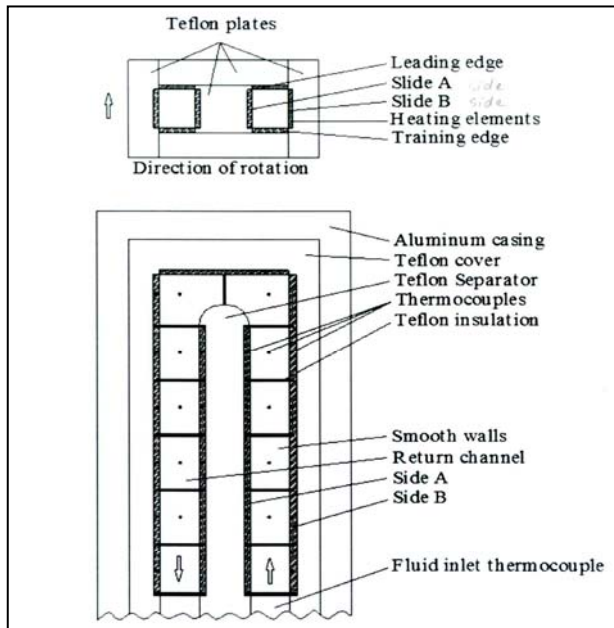

Fig 4. Heat transfer test model construction

2.2. Accuracy

An attempt will be made to provide an explanation of the inaccuracies and their impact on the air properties and then on the dimensionless parameters studied. There could be an error in temperature measurement. The sources of temperature errors are the initial calibration of the thermocouples, the e.m.f. measurements and the numerical curve fitting of the experimental temperature measurements. Another source of error could stem from flow rate measurement. Wattmeter, Rotational speed,

and physical dimensions, are among the sources of errors. It is decided, due to their importance, to concentrate on inaccuracies in fluid properties as well inaccuracies in dimensionless parameters.

2.2.1. Inaccuracies in Fluid Properties

Air being the coolant medium used in the present study, the error in its properties, namely, density, viscosity, thermal conductivity and specific heat at constant pressure were estimated.

This was done by using polynomial in terms of the fluid temperature which were included as part of the data processing program. However the pressure differentials encountered in this study were minor and the operating pressure tended to atmospheric pressure levels. Therefore, the approximation of the inaccuracies in these properties was largely based on the known errors in temperature measurements, i.e. $\pm 0.6 \,^{\circ}$C. These inaccuracies are shown in Table 2.1.

Tab 2.1 Estimated maximum percentage errors in the coolant fluid properties

Dimensionless parameters	Physical quantities	Maximum percentage error (%)
Nusselt Number	Nu	± 10.01
Reynolds number	Re	± 4.2
Prandtl number	Pr	± 0.5
Buoyancy parameter	$\beta . \Delta T_{w(z)}$	± 0.32
Rossby number	Ro	± 4.6
Eccentricity	ε	± 0.6

2.2.2. Inaccuracies in Dimensionless Parameters

The estimation of the maximum errors in the dimensionless parameters, equation 4, is presented in Table 2.2. These parameters are based on the maximum inaccuracies inherent in the variables making up each of these dimensionless parameters

Table 2.2. Estimation of the maximum percentage errors in the local values of the dimensionless groups

Coolant fluid properties	Physical quantities	Maximum percentage error (%)
Fluid density	ρ	± 0.30
Fluid viscosity	μ	± 0.20
Fluid thermal conductivity	k_f	± 0.25
Fluid sp. Heat at constant pressure	C_p	± 0.005
Fluid volume thermal expansion	β	± 0.16

3. Method of Data Evaluation

Each of the three physical situations was subjected to the same experimental program. The local heat transfer coefficient was calculated from Eq. (1):

$$q_{net} = h[A(T_w - T_b)] \tag{1}$$

where T_w, the local wall temperature on each copper plate and T_b, the local bulk mean coolant temperature respectively. For calculating local heat transfer coefficients (leading, trailing, side edges) used was made from the above equation. However, the local net heat transfer rate was the electrical power generated from the heaters minus the heat loss outside the test module. In other words:

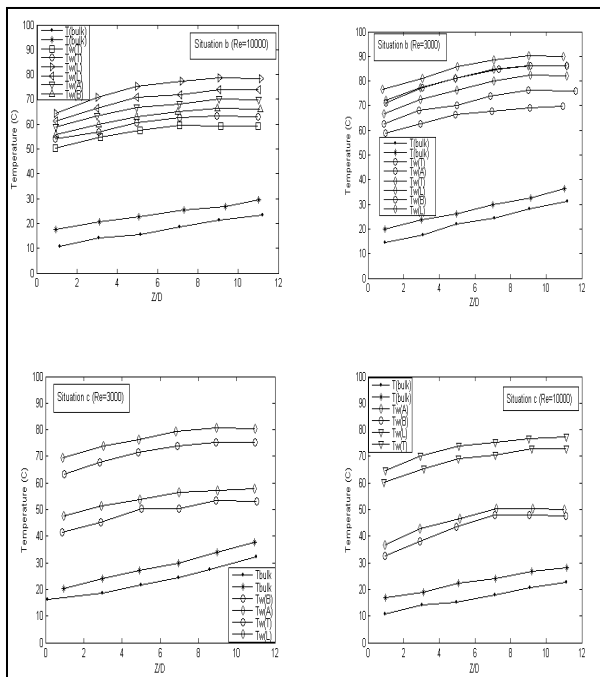$$q_{net} = q_{heater} - q_{loss} \qquad (2)$$

The electrical power generated from the heater was determined from the measured heater resistance and voltage on each wall of the test module. The effect of the local wall temperature variation on the local heater resistance was estimated to be not more than 2 percent. This estimation was included in the data reduction process. The effect of axial wall conduction between copper sections on the local heat transfer rate was less than 2 percent. Again, this is included in the data analysis. Tests were performed in order to determine the total heat loss from each of the test model walls without coolant flow but with rotation. For steady state, the loss calibration was performed by supplying power to the test model. This was achieved for several different power inputs to obtain the relation between the total heat loss from each surface and the corresponding surface temperature. Having determined the axial variation of heat flux, the fluid bulk temperature was calculated by means of an enthalpy balance.

Thus, from knowledge of heat flux, wall temperature and fluid bulk temperature, the heat transfer coefficient distribution along the duct could be calculated and presented non-dimensionally in terms of a local Nussle number on the leading and trailing edges of the channel.

Fig 5. Surface and coolant temperature variations along axial location (situations b and c)

All the local wall temperatures were read from the thermocouples output of each copper plate. The local bulk mean coolant temperature was computed from the local net heat input to the coolant flow through each of heated edges. The local bulk mean temperature was determined locally. The determination of the local bulk mean temperature was done by marching along the test module calculating the temperature rise due to the local net heat input to the coolant. All the aforementioned local temperatures were inserted into Eq. (1) for data evaluation process. The estimation began at the inlet of the heated test module where the coolant temperature was measured by a single thermocouple. The local bulk mean coolant temperature for individual heated surfaces was calculated by averaging the inlet and exit calculated bulk mean coolant temperature for each set of four (even and odd) heated walls. Typical variations of local wall to bulk mean coolant temperature along the test module for two different surface heating conditions, situations (b) and (c) are shown in Fig. 5. For a given flow Reynolds number, the Nussle number was calculated after extracting heat transfer coefficient from Eq. (1). Reynolds and Nussle number evaluations were based on average value. In other words, the physical properties were evaluated at the average of the inlet and outlet bulk mean coolant temperatures.

In order to diminish the influence of flow Reynolds number on the heat transfer coefficient with rotation, it is customary to normalize the Nussle number by the Nussle number calculated for fully developed turbulent flow in smooth walled tubes. In other words, to benefit from Dittus-Boelter [22]:

$$\frac{Nu_{local}}{Nu_\infty} = \frac{(hD/k)}{\left[0.023 \, Re^{0.8} \, Pr^{0.4}\right]} \qquad (3)$$

The physical properties for coolant (air) at the temperature range in the present experimental work used to calculate Prandtl number. It is found that Pr = 0.72. The local wall-to-coolant temperature difference will effect on uncertainty due to the local heat transfer coefficient. Also, another parameter influences the aforementioned uncertainty is the net heat input to the coolant flow from individual heated copper plate. The uncertainty of the local heat transfer coefficient increases with decreasing local wall temperature minus local bulk temperature and also with the net heat input.

Also, the uncertainty increases for low heat inputs, for example, low Reynolds numbers and on the leading surfaces. All the abovementioned uncertainties were estimated by the methods introduced by Kline and McClintock [23]. To summarize, the uncertainty in the Nussle number was found to be less than 7 percent for high Reynolds number (greater than 10,000). As one may guess, the highest uncertainty is attributed to the local heat transfer coefficient. For example, the maximum uncertainty could be even up to 25-30 percent for the lowest heat transfer coefficient on the leading edge of the test module at the lowest Reynolds number experimented.

4. Parameters Influencing Local Heat Transfer Coefficient

For fully developed turbulent forced convection flow in a tube, the Nussle number is a function of Reynolds (Re) and Prandtl (Pr) numbers. As already demonstrated by many researchers, such as Wagner et al., [14], the characteristics of forced convection heat transfer mechanism in the fully developed channel flow is altered by the rotation number (Coriolis forces) as well as wall-to-coolant temperature difference (centripetal buoyancy). Consequently, the Nussle number may be correlated by a number of parameters influencing the forced convection heat transfer mechanism. The functional relationship may be shown to be of the form:

$$Nu = \phi\left(\frac{R_{mean}}{D}, \frac{Z}{D}, \text{Re}, \text{Pr}, Ro, \frac{(T_w - T_b)}{T_w}\right) \qquad (4)$$

as mentioned already Pr = 0.72. Experiments were accomplished for four different Reynolds numbers Re=3000, 5000, and 30,000 and three different rotational speeds Ω=0,450, and 850 rpm, respectively. The rotational numbers varied from Ro= 0.0 up to 0.356. The effect of local surface heating conditions on the local heat transfer coefficient was investigated. The experiments carried out for one uniform wall temperature condition, situation (a) and two non-uniform wall temperature conditions, namely, situations (b) and (c), respectively. The results of all experiments were evaluated on a local basis by varying each parameter while holding the remaining parameters constant. Here are the influences of individual variables on the local heat transfer coefficients investigated during the present work.

(i) Influence of rotational speeds on local heat transfer coefficient

The averaged heat transfer results are given here as the axial distributions of heat transfer ratios.
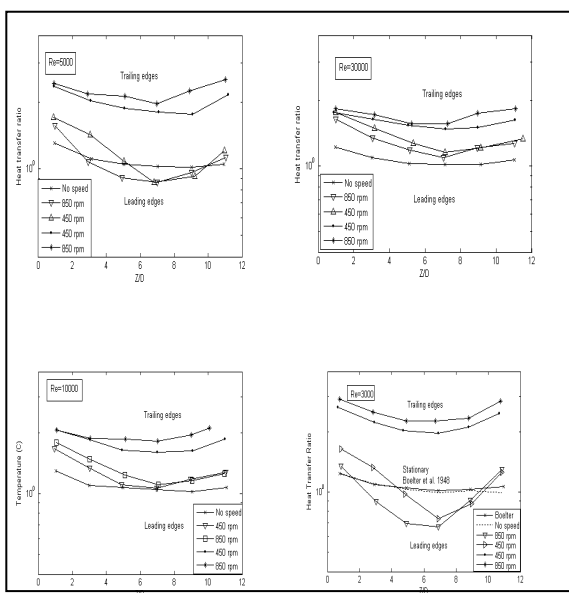

Fig 6. Influence of rotational speed on heat transfer ratio for leading and trailing edges

Fig. 6 shows the influence of rotational speed on the leading and trailing edges heat transfer ratio distributions for the Reynolds number varying 3000, 5000, 10,000 and 30,000, respectively, for the case of uniform heat flux, situation (b). For comparison purposes, the results for these tests corresponding stationary tests are also shown.

It is worth to note that the non-rotational heat transfer ratios on the leading and trailing edges are close to each other for the four Reynolds numbers investigated. As is clear from the figure, the non-rotational heat transfer ratio decreases monotonically from 1.6 near the thermal entry length of the first passage to about 1.0 near the downstream $\left(\frac{Z}{D} = 8.75\right)$ and then increases very little

near axial position downstream $\left(\frac{Z}{D} = 10.75\right)$ due to

flow entering the sharp 180 degree bend. Results of Dittos Bolter et al., [22] for fully developed forced convection flow is given on the figure. One can possibly appreciate the agreement between present results due to non-rotational tests and Dittos Bolter et al., [22] correlation.

However, with a Reynolds number of 3000 and rotational speed of 850 rpm the heat transfer ratios increases by 2-3 times from the trailing edges in comparison to the heat transfer ratios from the non-rotational condition.

The heat transfer ratio on the leading edge decreases sharply from the entry length to about 65 percent of the non-rotational value downstream $\left(\frac{Z}{D} = 5.75\right)$ and then

increases sharply at the larger downstream location. It is implied that the trailing edge heat transfer coefficient could be 3-4 times higher than that of the leading edge because of rotational speed of 850 rpm and Reynolds number of 3000.

However, as seen from Fig. 6, the difference of the heat transfer coefficients between the trailing and leading edges diminishes with decreasing rotational speed from 850 rpm to 450 rpm.

It is revealed from the figure that the difference of the heat transfer coefficients between the trailing and leading edges with increasing Reynolds number (Re =3000 to 30,000). It is also seen that the heat transfer ratio on the leading edge can be higher, expecting to be lower than that of the stationary value for Reynolds number higher than Re= 10,000.

(ii) Influence of Reynolds number on local heat transfer coefficient

The influence of Reynolds number on the leading and trailing edges heat transfer ratio for two different rotational speeds is shown in Fig. 7.

The figure shows the situation of uniform heat flux. The trailing heat transfer ratio increases up to 2-3 times with decreasing Reynolds number (reducing Re = 30,000 to 3000 for a fixed rotational speed of 850 rpm). In the contrary to trailing surface, the leading surface heat

transfer ratio decreases up to 0.5 with decreasing Reynolds number from 30,000 to 3000.
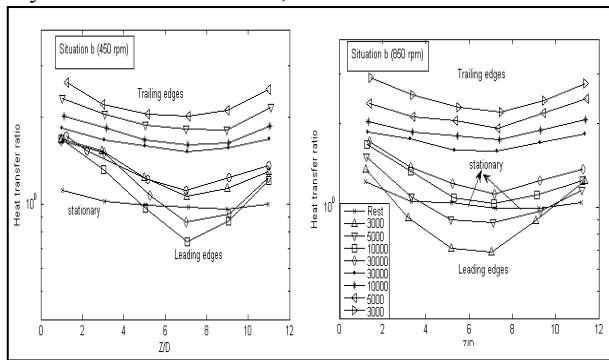

Fig 7. Influences of Reynolds number on heat transfer ratio for different rotational speeds

However, the heat transfer ratio decreases and then increases again near the end region of the channel. It is worth to note that similar behaviors are also achieved for a rotational speed of 450 rpm.

It is understood that the rotation has a significant effect on the trailing and leading edge heat transfer coefficients at a lower Reynolds number but the effect diminishes at a higher Reynolds number.

The Reynolds number is proportional to the stream-wise inertia force while the rotational speed generates the cross-stream secondary flow due to the Coriolis force. The ratio of the strength of the Coriolis to inertia, cross-stream to stream-wise, decreases with increasing Reynolds number for a fixed rotational speed. Consequently, the influence of rotation on the local heat transfer reduces at a higher Reynolds number for a fixed rotational speed.

Therefore, it is not surprising that, in some circumstances, the heat transfer ratio on the leading surface could be higher than that of the non-rotating value at higher Reynolds number flows.

(iii) Influence of non-uniform wall temperature with varying rotational number on local heat transfer coefficient

It is clear by now that the heat transfer coefficients on the leading and trailing edge of a rotating channel with radial outward flow direction can be altered by the rotational speed (Coriolis force) as well as Reynolds number.

Fig. 8 shows the effect of non-uniform wall temperature on the leading and trailing edge heat transfer ratio for the investigated rotational numbers. Three different situations of heating conditions are presented: (a) four walls uniform temperature, (b) four wall uniform heat flux, and (c) leading and trailing hot but two sides wall kept cold. One should note that the test results for the non-rotational heat transfer ratios on the trailing and leading surface for the three situations of surface heating conditions are almost about the same. Consequently, the non-rotational heat transfer ratios are shown as a single curve for the purposes of comparison (see Fig. 8 for clarity).
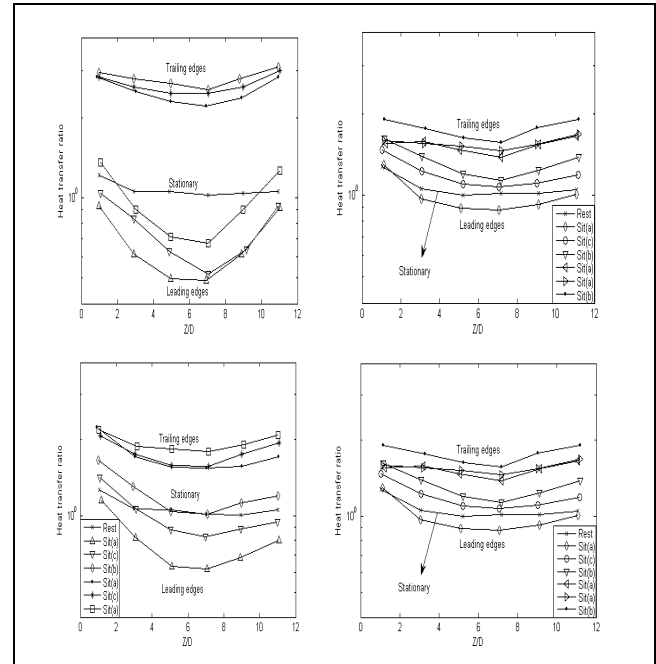

Fig 8. (a) Influences of surface heating condition on heat transfer ratio for situations (a), (b), and (c)

For the situation (a) of four wall uniform temperature, the difference of the heat transfer coefficients between the rotating and non-rotating conditions on the leading and trailing edges is attributed to both the increasing strength of the secondary cross-stream flow vortices due to the Coriolis force and the centripetal buoyancy. Han et al., [4] also came to the same conclusions. The higher trailing surface heat transfer coefficients are because firstly, the coolant impingement due to rotation on the trailing edge creates thinner boundary layer, and secondly, the coolant profile distortion due to rotation produces a stronger centripetal buoyancy-induced wall turbulence near the destabilized trailing surface thin boundary layer.

However, the decreases in heat transfer coefficients near the inlet of the channel on the leading edges is due to a thicker stabilized boundary layer, and the subsequent increases in heat transfer coefficients near the end of the channel is attributed to the stronger centripetal buoyancy-induced, destabilized wall turbulence boundary layer. The abovementioned statements are the typical combined influences of Coriolis and buoyancy forces due to rotation on the leading and trailing edges of a square channel with four wall uniform temperature and with coolant outward flow direction. For the situation (b) of four walls uniform heat flux, the results show that the trailing edge heat transfer ratio is 6-15 percent higher than that of situation (a) but not for the larger rotational number. However, the results show that the leading edge heat transfer ratio for situation (b) is 20-80 percent higher than that of situation (a). For the situation (c) of leading and trailing hot but two sides wall cold, the trailing edge heat transfer ratio is almost about the same as the situation (a). Again, the leading edge heat transfer ratio of situation (c) is 10-40 percent higher than situation (a) for all experimented rotational

numbers. Figure 8 (a) & (b) show that the heat transfer ratio decreases toward the middle of the test section and then increases again.
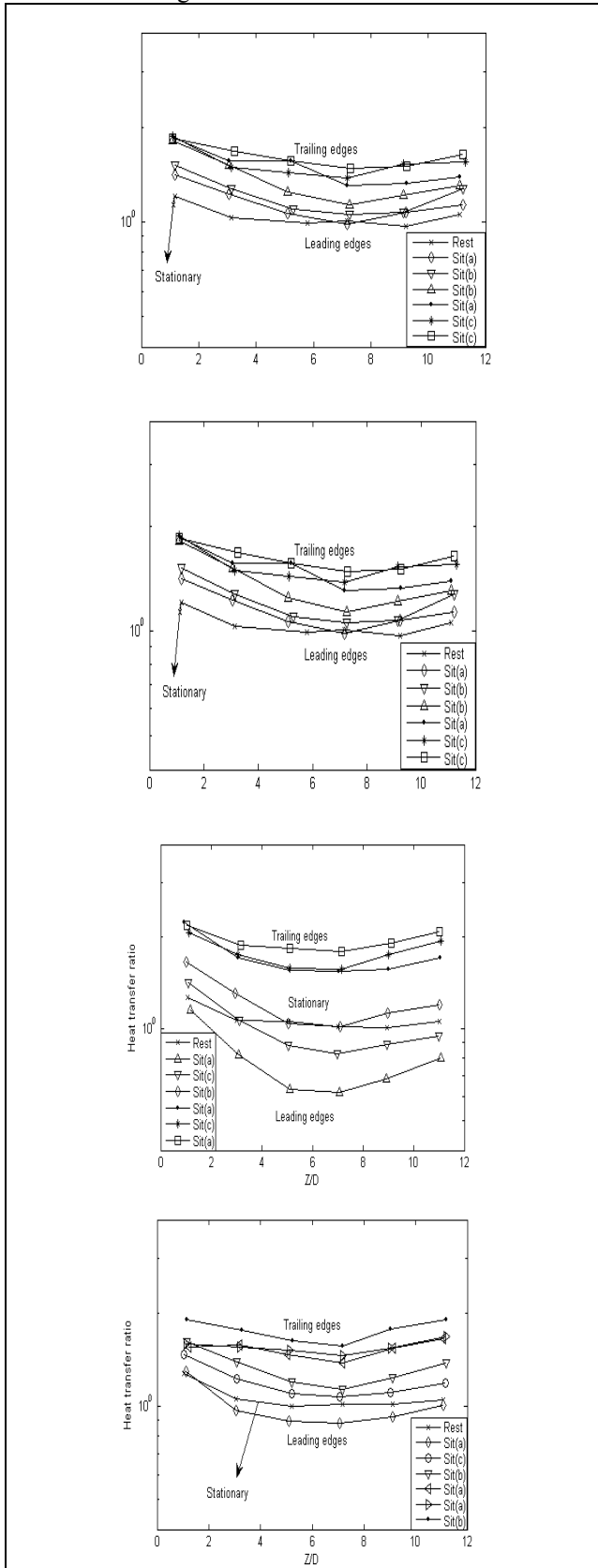

Fig 8. (b) Influence of surface heating condition on heat transfer ratio for situations (a), (b), and (c)

This is due to the fact that at the entry to the test section a relatively cooler coolant enters.

As it moves towards the middle of test section, the thermal boundary layer build up and therefore a thicker boundary layer developed and established. The increase in heat transfer ratio near the end of the channel is attributed to the strong centripetal buoyancy-induced, destabilized wall turbulence boundary layer. The temperature distribution on the trailing edge is lower than leading and sidewall edges. This in turn results in a cooler coolant near the trailing edge. The cooler coolant is accelerated due to centrifugal buoyancy and a thinner boundary layer is created near the trailing edge. Fig. 8 (b) shows that the trailing edge heat transfer coefficients for situation (b) are slightly higher than situation (a) and the leading edge heat transfer coefficients for situation (b) are not as low as situation (a). Fig. 8 shows that the trailing edge heat transfer coefficients for situation (c) are slightly lower than situation (a) and the leading edge heat transfer coefficients for situation (c) are higher than situation (1). The next section focuses on correlating experimental data.

5. Results and Discussion

The convective heat transfer coefficients on the leading and trailing edges of a rotating channel with radial outward flow direction can be altered by rotational number (Coriolis force) as well as the surface heating condition (local buoyancy force).

Fig. 9 (a) shows the variation of heat transfer ratio with rotational number at some axial locations for the three different surface heating conditions investigated. (1) Situations (a), (b), and (2) situations (a) and (c). Included in the figure are the experimental results from Wagner et al., [14] for the case of uniform wall temperature for comparison. The results show that the present heat transfer ratio on the trailing and leading edge for the situation of uniform wall temperature condition agree with those of Wagner et al., but not for axial location $\left(\dfrac{Z}{D}=5\right)$. This approves the fact that the

trailing edge heat transfer ratio increases with an increasing rotational number. However, the leading edge heat transfer ratio decreases and then increases with an increasing rotational number for the case of uniform wall temperature condition. At the axial location mentioned above, the leading edge heat transfer ratios for the present work are much lower than that of Wagner et al., [14]. The difference may be caused by the flow inlet condition used in each study. A fully developed slow entry length for this study versus a sharp developing flow entrance for the Wagner et al., [14]. The fully developed flow profile with a thicker boundary layer can be easily influenced by the Corilis force than the developing accelerating flow with a thinner boundary layer. Consequently, the leading edge heat transfer ratios of the present work are much lower. The non-uniform wall temperature on both the leading and

trailing edges creates unequal local buoyancy forces that alter the heat transfer coefficients.
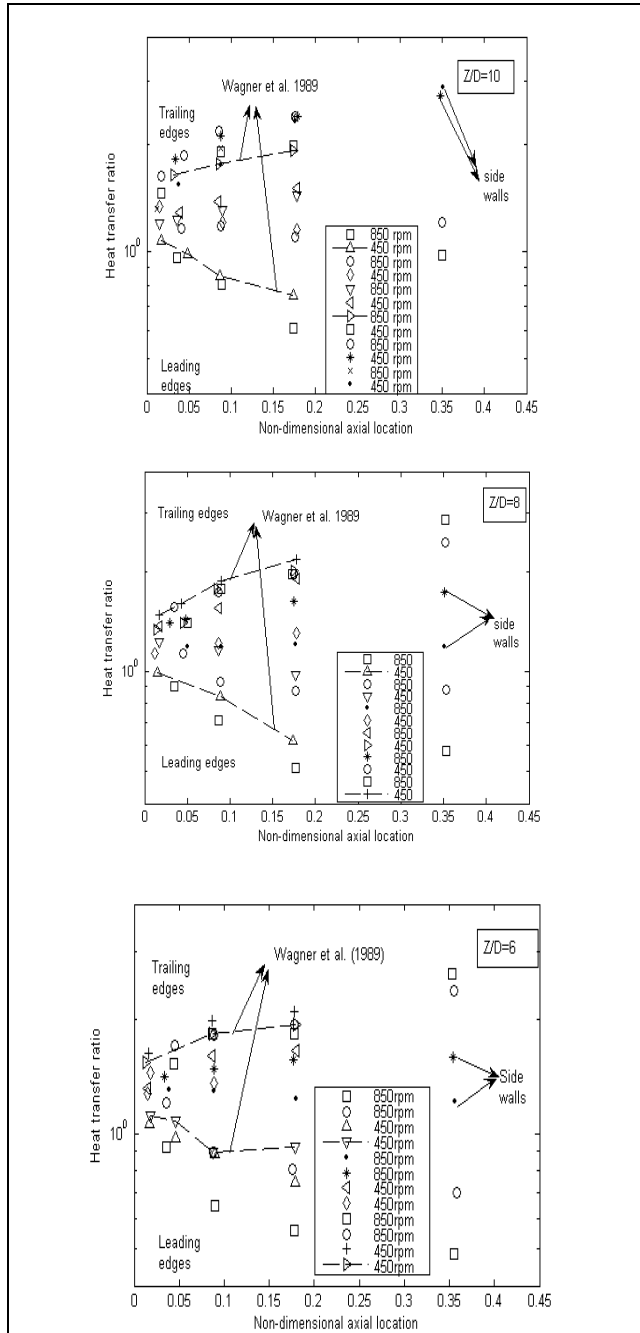

Fig. 9 (a) Influence of rotational number on heat transfer ratio at selected axial locations for situations (a) and (b)

Fig. 9 (a) shows that the trailing surface heat transfer ratios for situation (b) are 15-25 percent higher than that for situation (a), whereas, the leading edge heat transfer ratios for situation (b) are 40-85 percent higher than that for situation (a). Fig. 9 (b) suggests that the trailing edge heat transfer ratios for situation (c) are about the same situation (a), but the leading edge heat transfer ratios for situation (c) are 25-40 percent higher than that for situation (a). It is obvious that the local buoyancy force interacts with the Coriolis force and enhances the effect of the rotational number on the trailing edge heat

transfer coefficients but reduces the effect of the rotation number on the leading edge heat transfer coefficients. Fig. 9 (a) also shows that the heat transfer ratio from two side walls (side walls A and B) are about the same for situation (a) and about 20-30 percent higher than the non-rotating results.

The results also show that the heat transfer ratio from two sides wall are about the same for situation (b) but about 20-50 percent higher than that for situation (a). Fig.10 shows the variation of the channel averaged Nussle number ratio with rotational number for (1) situations (a) and (b) and (2) situations (a) and (c). The channel averaged Nussle number ($Nu_{channel\ averaged}$) on the leading edge or trailing edge, side wall A, side wall B is the average value of the entire leading edge or trailing edge, side wall A, side wall B local Nussle number (Nu_{local}) from the $\left(\dfrac{Z}{D}=1\right)$ to $\left(\dfrac{Z}{D}=11\right)$.
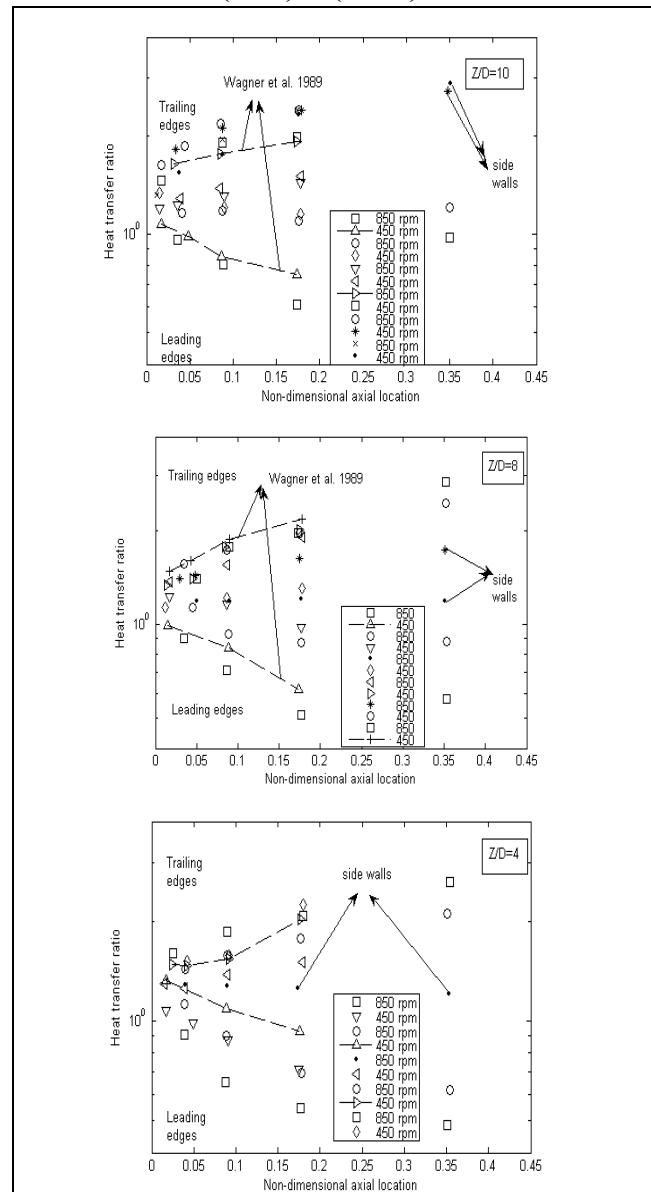

Fig 9. (b) Influence of rotational number on heat transfer ratio at selected axial locations for situations (a) and (b) leading and trailing edges
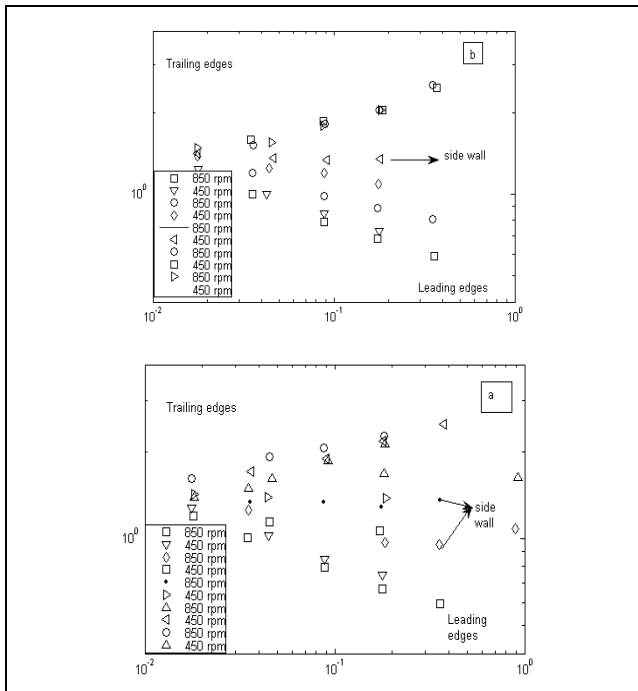
Fig. 10 Influence of rotational number on average heat transfer ratio for situations (a) and (b), as well as (c)

The results show that for situation (a) uniform wall temperature, the channel averaged Nusselt number ratio on the leading edge increases from 1.4 to 2.6 when the rotational number changes from a lower value to a maximum value of 0.356, where as the corresponding channel averaged Nusselt number ratio on the leading edge decreases from 1.3 to 0.7 and the channel averaged Nusselt number ratio from side wall A and side wall B are alike over the range of rotational numbers experimented. Again, the influence of non-uniform wall temperature is firstly, to increase the leading edge average heat transfer coefficients for situations (b) and (c) compared to situation (a) and secondly, to increase the trailing edge average heat transfer coefficients for situation (b) and finally to increase the side wall heat transfer coefficients for situation (b).

6. Conclusions
The experiments have been accomplished for rotating number from zero to 0.356 and Reynolds number from 3000 to 30,000.The main findings are:1The decreased or increased heat transfer coefficient on the leading or trailing surface are due to formation of the cross-stream and centripetal buoyancy-induced flows caused by rotation. 2 For a fixed rotational speed, the effect of rotation on the trailing and leading surface heat transfer ratio increases with decreasing Reynolds number. This is caused because of the relative strength of the Coriolis to inertia force enhances at a lower Reynolds number.
3 The non-uniform wall temperature for the situations (b) and (c) creates unbalanced buoyancy forces between the leading and trailing surface. This in turn reduce the quantities of cross-stream flow between the leading and trailing surfaces and degrades the effect of rotation on the local leading and trailing heat transfer coefficient.

4 The trailing surface heat transfer coefficients for non-uniform wall temperature (situation b) are slightly higher than that for uniform surface temperature (situation a). The leading surface heat transfer coefficients for non-uniform wall temperature (situations b and c) are much higher than that of uniform wall temperature (situation a). This implies that the difference between the leading and trailing heat transfer coefficient with non-uniform wall temperature becomes smaller compared to the uniform wall temperature situation.
5 The trailing surface heat transfer ratios for non-uniform wall temperature condition (situation b) are 15-25 percent higher than that for uniform surface temperature (situation a) at a given rotational number. However, the leading surface heat transfer ratios for situations (b) and (c) are up-to 80 percent higher and up-to 40 percent, respectively, than that for uniform wall temperature (situation a) for a given rotational number.

References
[1] Han, J.C., Glicksman, L.R., & Rohsenow, W.M., *"An Investigation of heat transfer and friction for rib-roughened surfaces"*, Int.J. Heat and Mass Transfer, Vol. 21, 1978, PP. 1143-1156.

[2] Han, J.C., *"Heat transfer and friction in channels with two opposite rib-roughened walls"*, ASME Journal of Heat Transfer, Vol. 110, 1984, PP. 774-781.

[3] Han, J.C., *"Heat transfer and friction characteristics in rectangular channels with rib tabulators,"* ASME Journal of Heat Transfer, Vol. 110, 1988, PP. 321-328.

[4] Han, J.C., Zhang, Y.M., & Lee, C.P., *"Augmented heat transfer in square channels with parallel, crossed, and V-Shaped angled ribs"*, ASME Journal of Heat Transfer, Vol. 113, 1991, PP. 590-596.

[5] Mori, Y., Fukada, T., & Nakayama, W., *"Convective heat transfer in a rotating radial circular pipe (2nd Report),"* International Journal of Heat Mass Transfer, Vol. 14, 1971, PP. 1807-1824.

[6] Clifford, R.J., Morris, W.D., & Harasgama, S.P., *"An experimental study of local and mean heat transfer in a triangular-sectioned duct rotating in the orthogonal mode"*, ASME Journal of Engineering for Gas Turbines and Power, Vol. 106, 1984, PP. 661-667.

[7] Morris, W.D., Harasgama, S.P., & Salemi, R., *"Measurements of turbulent heat transfer on the leading and trailing surfaces of a square duct rotating about an orthogonal axis"*, ASME paper No. 88-GT-114, 1984.

[8] Morris, W.D., & Ghavami-Nasr, G., *"Heat transfer measurements in rectangular channels with orthogonal mode rotation,"* ASME paper No. 90-GT-138, 1990.

[9] Morris, W.D., & Salemi, R., *"An attempt to experimentally uncouple the effect of coriolis and buoyancy forces on heat transfer in smooth circular tubes which rotate in the orthogonal mode,"* ASME paper No. 91-GT-17, 1991.

[10] Morris, W.D., & Farhadi Rahmat-Abadi, K., *"Convective heat transfer in rotating ribbed tubes,"* Int. J. of Heat and Mass Transfer, Vol. 11, 1996, PP. 2253-2266.

[11] Soong, C.Y., Lin, S.T., & Hwang, G.J., *"An experimental study of convective heat transfer in radially rotating rectangular ducts,"* Trans. ASME, Vol. 113, 1991, PP. 604-611.

[12] Liou, T.M., & Hwang, J.J., *"Developing heat transfer and friction in a ribbed rectangular duct with flow separation an inlet"*, Int. J. of Heat and Mass Transfer, Vol. 114, 1992, PP. 565-573.

[13] Wagner, J.H., Kim, J.C., & Jognson, B.V., *"Rotating heat transfer experiments with turbine airfoil internal passages"*, ASME paper No. 86-GT-133, 1986.

[14] Wagner, J.H., Johnson, B.V., & Hajek, T.J., *"Heat transfer in rotating passages with smooth walls and radial outward flow"*, ASME paper No. 89-GT-272, 1989.

[15] Wagner, J.H., Johnson, B.V., & Kopper, F.C., *"Heat transfer in rotating serpentine passages with smooth walls"*, ASME paper No. 90-GT-331, 1990.

[16] Wagner, J.H., Johnson, B.V., Graziani, R.A., & Yeh, F.C., *"Heat transfer in rotating serpentine passages with trips normal to the flow"*, ASME paper No. 91-GT-265, 1991.

[17] Matsuda, H., Ikeda, K., Nakata, Y., Otomo, F., Suga, T., & Fukuyama, Y., *"A new thermo chromic liquid crystal temperature identification technique using color space interpolations and Its application to film cooling effectiveness measurements"*, Proceeding of PSFVIP-2, PF053, 1999.

[18] Saeki, H., Ito, S., Matsuda, H., & Okamura, T., (1999), *"Heat transfer measurements on turbine nozzle using liquid crystals"*, International Gas Turbine Congress 99 Kobe, 1999, TS-47, PP. 607-613.

[19] Jackson, J.B. A., Neto, A.C., Whellens, M., & Audus, *"Gas turbine performance using carbon dioxide as working fluid in closed cycle operation"*. ASME, 2000-GT-153, 2000.

[20] Saeki, H., & Fukuyama, Y., *"Heat transfer measurements on a gas turbine blade for ACRO-GT-2000"*, ISROMAC-9, Paper HT-ABS-025 2002.

[21] Shoko Ito, Saeki, H., & Inomata, A. *"Conceptual design and cooling blade development of 1700 ˚C Class High-Temperature gas turbine"*, J. Eng. Gas Turbine and Power, Vol. 127, April 2005, PP. 358-368.

[22] Boelter, L.M.K., Young, G., & Iverson, H.W., *"An investigation of aircraft heaters-distribution of heat transfer rate in the entrance section of a circular tube"*, NACA TN 1451, Washington, 1948.

[23] Kline, S.J., & McClintock, F.A., *"Describing uncertainties in single-sample experiments,"* Mechanical Engineering, 1953, PP. 3-8.

Nomenclature

A: heat transfer area

D_h: hydraulic diameter

h: heat transfer coefficient

K: coolant thermal conductivity

L: heated channel length

Nu: Nusselt number

Nu_∞: Nusselt number in fully developed forced convection tube flow

Pr: Prandtl number

q: heat generation rate

q_{loss}:   heat loss rate

q_{net}:   net heat transfer rate

R: rotating radius

R_{mean}: mean rotating radius

Re: Reynold number

Ro: Rotational number

T_b: local bulk mean coolant temperature

T_{bi} : inlet bulk mean coolant temperture

T_w: local wall temperature

$T_{w\,(A)}$: local wall temperature of side wall A

$T_{w\,(B)}$: local wall temperature of side wall B

$T_{w\,(L)}$: local wall temperature of leading edge

$T_{w\,(T)}$: local wall temperature of trailing edge

V: mean coolant velocity

Z: axial location along heated channel

$(T_w - T_b)/T_w$: coolant-to-wall density ratio based on local bulk mean coolant temperature

$(T_w - T_{bi})/T_w$: coolant-to-wall density ratio based on inlet bulk mean coolant temperature

Ω: rotational speed